Progress In Electromagnetics Research C, Vol. 155, 235–244, 2025

PIER C

(Received 4 March 2025, Accepted 11 May 2025, Scheduled 18 May 2025)

Calculation and Analysis of RCS of Metamaterial Coated Composite Structure

Osman M. Alsemaid*, Elased Sulieman Saad, and Ahmed Awad Babiker

Karary University, Sudan

ABSTRACT: The RCS of a composite target composed of two geometries, namely elliptical cylinder plus elliptical cone, is calculated and analyzed in this paper. To get the RCS for the target shape, RCSs of both the elliptical cylinder and elliptical cone are calculated and analyzed before and after coating them with a designed metamaterial. Matlab and CST Simulator are used to evaluate the performance and prove the effectiveness of the metamaterial coating in reducing the RCS of the composite structure, using specially created metamaterials. This search lowered RCS across a wide frequency range of 2 to 400 GHz, which is done through specially designed metamaterials.

1. INTRODUCTION

Conducting structures' backscattering echo width, if it is wide, cannot be disregarded. Such conducting objects are covered with radar-absorbing compounds to lessen scattering. Since five decades ago, numerous research have been published in the literature. An precise solution to the scattering from a right circular cylinder covered with dielectric material was attempted in classical works by Wait [1], Wang [2], and numerous others. Emile Leonard Mathieu's 1868 investigation of the vibration modes of an elliptic membrane produced the Mathieu Function and its characteristics, which served as the foundation for scattering analyses of elliptical geometries, such as elliptical cylinders. Mathieu functions provide a straightforward way to express the echo width of an elliptical cylinder that conducts properly [3].

Dealing with the field both within and outside the structure is essential for a conducting structure covered in dielectric material. By taking into account diffraction from a penetrable ribbon, Yeh [4] was able to solve the scattering from a dielectric object. Richmond [5] calculated a conducting elliptic cylinder covered with a homogeneous dielectric material's scattering characteristics. The boundary condition in the dielectric-free space interface has been defined using Galerkin's approach, and Mathieu functions are employed to do numerical calculations. The scattering characteristics of a dielectric-covered impedance elliptic cylinder were computed by Sebak [6]. For both TM and TE polarizations, the field distribution in each region was determined using impedance boundary conditions.

Caorsi et al. [7] have given an exact solution to the electromagnetic scattering by a multilayered dielectric infinite cylinder of elliptic cross section. It is assumed that the interface is non-magnetic and lossless. The dispersed field from an elliptic cylinder covered with confocal dielectric and illuminated by a point source was calculated by Ragheb et al. [8]. Additional generic solutions, which can be either confocal or non-confocal, were proposed for covered elliptic cylinder scattered fields [8].

It is observed that radial and angular Mathieu functions are used to find the precise solution for the dispersed field from an elliptic cylinder. The Mathieu function differential equation yields the angular Mathieu function, while the modified Mathieu function differential equation yields the radial Mathieu function [9]. The expansion coefficients and eigenvalues, in addition to the radial and angular Mathieu functions and their normalized factors, are important components of an elliptic cylinder's dispersed field. The radar cross-section (RCS) of a covered conducting elliptic cylinder is calculated analytically in this work. The field within and outside the cylinder is computed using the addition theorem, which yields scattering coefficients and angular and radial Mathieu functions. Analysis is done on how coating metamaterial characteristics affect cylinder RCS.

The results of a rigorous solution of this scattering problem have been contrasted with the physical optics approximation for the backscattering radar cross section of a circular semi-infinite cone by Siegel et al. [10]. For both large and small cone angles, they discovered a good agreement between the two results. Therefore, it is reasonable to believe that the physical optics approximation is sufficiently precise for calculating a semi-infinite elliptic cone's backscattering cross section.

Blume and Kahl provided a solution to this issue in a previous paper [11]. Because of the coordinate system used to interpret the results, it can be challenging to explain the scattered geometry. As will be demonstrated, if the geometry is described by the two extreme flare angles of the elliptic cone, the conclusion becomes extremely straightforward. It becomes feasible to compare the outcome directly to that of the circular cone. The bistatic radar cross section of an elliptic cone will be computed if the receiver is positioned inside one of the cone's two symmetry planes.

* Corresponding author: Osman M. Alsemaid (osman98@yahoo.com).

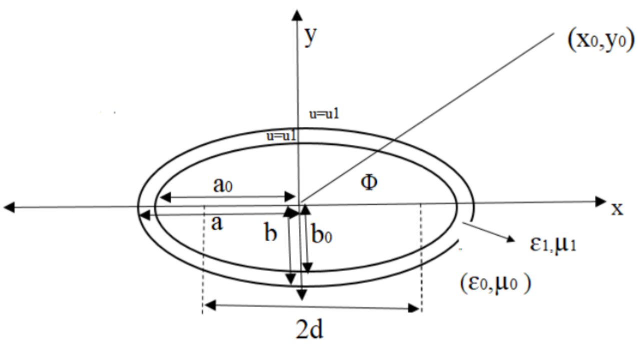

FIGURE 1. Geometry of elliptic cylinder.

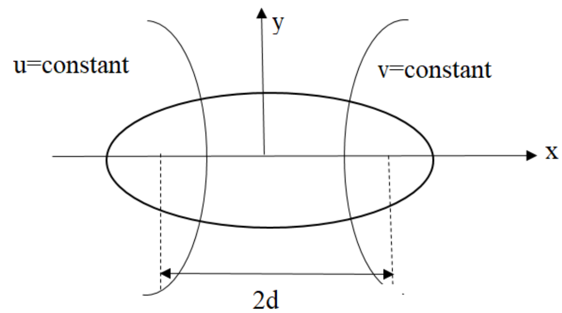

FIGURE 2. Elliptic cylinder coordinates.

The purpose of this study is to analyze the electromagnetic wave scattering of the conical and cylindrical shapes independently, to investigate a shape made up of both shapes using the principle of superposition, to analyze the RCS of the shape if it is constructed out of perfect electric conductor (PEC) and covered with a metamaterial developed in [12], and the effect of this metamaterial on RCS.

2. ANALYTICAL FORMULATION FOR ELLIPTIC CYLINDER SHAPE

Observe the cross section of an elliptic cylinder with infinite length (Fig. 1) in free space (ε_0, μ_0). With semi-major and semi-minor axes and semi-focal lengths of a_0, b_0, and d, respectively, it is assumed that a conducting elliptic cylinder serves as the core. An metamaterial (ε_1, μ_1) with the focal length at $x = \pm d$ is applied to the cylinder. The structure is excited by a line source at (x_0, y_0). The expression for the incident field is,

$$E_z^i = H_0^2(k_0(\varsigma - \varsigma_0)) \tag{1}$$

where H_0^2 is the Hankel function of second kind and zero order, and k_0 is the wave number of free space. Throughout the derivation, the incident field's temporal dependence is disregarded. The analytical method can be applied to elliptic cylinder scattering problems. As illustrated in Fig. 2, the Cartesian coordinate system (x, y, z) is transformed into an elliptic cylindrical coordinate system (u, v, z).

Ellipse is defined in the Cartesian coordinate system from [13] as:

$$\left(\frac{x}{a_0}\right)^2 + \left(\frac{y}{b_0}\right)^2 = 1 \tag{2}$$

where $a_0 > b_0$, eccentricity $e = d/a_0$, and semi-focal length $d = \sqrt{a_0^2 - b_0^2}$ are all less than or equal to 1. The relations are satisfied by the elliptical coordinate system,

$$x = d\cos v \cosh u; \quad y = d\sin v \sinh u; \quad z = z \tag{3}$$

where $0 \le v \le 2\pi$ and $0 \le u < \infty$. It is feasible to describe these coordinates in terms of (ξ, η, z) with $\xi = \cosh u$, $\eta = \cos v$, and $z = z$. Consequently, one has:

$$x = d\xi\eta, \quad y = d\sqrt{(\xi^2-1)(1-\eta^2)}, \quad z = z. \tag{4}$$

These are the expressions for semi-major and semi-minor axes:

$$a_0 = d\xi, \quad b_0 = d\sqrt{\xi^2 - 1} \tag{5}$$

In TM polarization, the electric field will only contain an E_z component. The incident electric field can be expressed as [3] using the Mathieu function.

$$E_z^i = \sum_{i=0}^{\infty} \frac{Ce_i(c,v_0)Ce_i(c,v)Re_i^{(1)}(c,u)Re_i^{(4)}(c,u_0)}{Ne_i(c)} + \sum_{i=0}^{\infty} \frac{So_i(c,v_0)So_i(c,v)Ro_i^{(1)}(c,u)Ro_i^{(4)}(c,u_0)}{No_i(c)} \tag{6}$$

where $Re_i^{(1)}$ and $Ro_i^{(1)}$ are radial Mathieu functions of the first kind which are odd and even. Ne_i and No_i are even and odd normalized factors, while $Re_i^{(4)}$ and $Re_i^{(4)}$ are even and odd radial Mathieu functions of the fourth kind. Even and odd types of angular Mathieu functions are represented by letters Ce_i and So_i.

Wave numbers $k_1 = k_0\sqrt{\varepsilon_r}$ and $c = c_d = k_1 d$ are found within the dielectric zone. This equation is valid only when the source is positioned ζ_0 from the center. The $Re_i^{(4)}(c, u_0)$ and $Ro_i^{(4)}$ phrases in (6) can be skipped if the incident wave is a plane wave. Thus, the scattered field can be expressed as,

$$E_z^s = \frac{2\pi}{j}\left(\sum_{i=-0}^{\infty} \begin{array}{l} X_i^{TM}Ce_i(c,v)Re_i^{(4)}(c,u) + \\ \sum_{i=0}^{\infty} Y_i^{TM}So_i(c,v)Ro_i^{(4)}(c,u) \end{array}\right) \tag{7}$$

The field inside the metamaterial region is given by

$$E_z^1 = \frac{2\pi}{j}\left(\begin{array}{l} \sum_{r=0}^{\infty}[P_r^{TM}Re_r^{(1)}(c_d,u) + Q_r^{TM}Re_r^{(2)}(c_d,u)]Ce_r(c_d,v) \\ + \sum_{r=1}^{\infty}[S_r^{TM}Ro_r^{(1)}(c_d,u) + T_r^{TM}Ro_r^{(2)}(c_d,u)]So_r(c_d,v) \end{array}\right) \tag{8}$$

where X_i^{TM}, $Y_i^{TM} P_i^{TM}$, $Q_i^{TM} R_i^{TM}$, and S_i^{TM} must be established by applying appropriate boundary conditions in order to estimate the scattering coefficients, for the extraction of u_0 and v_0 from ξ_0 ($\xi = \cosh u$) and $\eta_0(\eta = \cos v)$, respectively.

Applying boundary condition when $u = u1$:

$$E_z^i + E_z^s = \begin{cases} E_z^1 & u1 < u < u2 \\ 0 & else \end{cases} \tag{9a}$$

$$H_v^i + H_v^s = H_v^1, \quad H\ _z^i = H_z^s \tag{9b}$$

$$E_z^1 = 0 \tag{9c}$$

Applying boundary condition when $u = u2$

$$E_z^i = E_z^s \tag{10a}$$

$$H_z^i = H_z^s \tag{10b}$$

The unknown coefficients for a plane wave incident on an elliptic cylinder are computed by replacing (6) and (7) in (8).

$$\begin{aligned} Y_i^{TM} &= -\tfrac{So_i(c,v_0)Ro_i^{(1)}(c,u)}{Ro_i^{(4)}(c,u)No_i(c)} \\ X_i^{TM} &= -\tfrac{Ce(c,v_0)Re_i^{(1)}(c,u)}{Re_i^{(4)}(c,u)Ne_i(c)}; \end{aligned} \tag{11}$$

The RCS of an uncoated elliptical cylinder is given in [13] by:

$$\text{RCS} = \frac{16\pi^2}{k_0}\left[\sum_{i=0}^{\infty} j^i X_i^{TM} Ce_i(c,v) + \sum_{i=1}^{\infty} j^i Y_i^{TM} So_i(c,v)\right] \tag{12}$$

The tangential component of the magnetic and electric fields for a covered elliptic cylinder is constant across the metamaterials surface. When a conducting cylinder is present, the electric field becomes zero.

$$\begin{aligned} 0 =& \sum_{r=0}^{\infty} [P_r^{TM} Re_r^{(1)}(c_d,u_1) + Q_r^{TM} Re_r^{(2)}(c_d,u_1)] Ce_r(c_d,v) \\ &+ \sum_{r=1}^{\infty} [S_r^{TM} Ro_r^{(1)}(c_d,u_1) + T_r^{TM} Ro_r^{(2)}(c_d,u_1)] So_r(c_d,v) \end{aligned} \tag{13}$$

One can use Mathieu functions to

$$\int_0^{2\pi} Ce_i(c_d,v) So_r(c_d,v) dv = 0;$$

$$\int_0^{2\pi} Ce_i(c_d,v) Ce_r(c_d,v) dv = \pi$$

The result of multiplying (13) by $Ce_i(c_d,v)$ and $So_i(c_d,v)$, then integrating over 0 to 2π, is

$$\begin{aligned} T_r^{TM} &= -S_r \frac{Ro_r^{(1)}(c_d,u_1)}{Ro_r^{(2)}(c_d,u_1)} \\ Q_r^{TM} &= -P_r \frac{Re_r^{(1)}(c_d,u_1)}{Re_r^{(2)}(c_d,u_1)}; \end{aligned} \tag{14}$$

When one replaces (14) in (8), one obtains:

$$E_z^1 = \frac{2\pi}{j}\left(\begin{aligned} &\sum_{r=0}^{\infty} P_r^{TM}\left[\begin{aligned} &Re_r^{(1)}(c_d,u) - \\ &\tfrac{Re_r^{(1)}(c_d,u_1)}{Re_r^{(2)}(c_d,u_1)} Re_r^{(2)}(c_d,u) \end{aligned}\right] Ce_r(c_d,v) \\ &+ \sum_{r=1}^{\infty} [S_r^{TM}\left[\begin{aligned} &Ro_r^{(1)}(c_d,u) - \\ &\tfrac{Ro_r^{(1)}(c_d,u_1)}{Ro_r^{(2)}(c_d,u_1)} Ro_r^{(2)}(c_d,u) \end{aligned}\right] So_r(c_d,v) \end{aligned}\right) \tag{15}$$

With boundary condition applied, $E_z^i + E_z^s = E_z^1$, one has

$$\begin{aligned} &\left(\sum_{i=0}^{\infty} \tfrac{Ce_i(c,v_0)Ce_i(c,v)Re_i^{(1)}(c,u_2)Re_i^{(4)}(c,u_0)}{Ne_i(c)}\right) + \\ &\left(\sum_{i=0}^{\infty} X_i^{TM} Ce_i(c,v) Re_i^{(4)}(c,u_2)\right) = \\ &\sum_{r=0}^{\infty} P_r^{TM}\left[Re_r^{(1)}(c_d,u_2) - \tfrac{Re_r^{(1)}(c_d,u_1)}{Re_r^{(2)}(c_d,u_1)} Re_r^{(2)}(c_d,u_2)\right] \\ &Ce_r(c_d,v) \end{aligned} \tag{16a}$$

$$\begin{aligned} &\left(\sum_{i=0}^{\infty} \tfrac{So_i(c,v_0)So_i(c,v)Ro_i^{(1)}(c,u_2)Ro_i^{(4)}(c,u_0)}{No_i(c)}\right) + \\ &\left(\sum_{i=0}^{\infty} Y_i^{TM} So_i(c,v) Re_i^{(4)}(c,u_2)\right) = \\ &\left(\sum_{r=1}^{\infty} [S_r^{TM}\left[\begin{aligned} &Ro_r^{(1)}(c_d,u_2) - \\ &\tfrac{Ro_r^{(1)}(c_d,u_1)}{Ro_r^{(2)}(c_d,u_1)} Ro_r^{(2)}(c_d,u_2) \end{aligned}\right] So_r(c_d,v)\right) \end{aligned} \tag{16b}$$

For the sake of clarity, even and odd terms are written separately here.

After integrating over 0 to 2π and multiplying (16b) and (16a) by $Ce_i(c,v)$, one obtains

$$\begin{aligned} \sum_{r=0}^{\infty} P_r^{TM} Ae_{r,i} R1_r =& \left(Ce_i(c,v_0) Re_i^{(4)}(c,u_2) Re_i^{(4)}(c,u_0)\right) \\ &+ X_i^{TM} Re_i^{(4)}(c,u_2) Ne_i(c) \end{aligned} \tag{17}$$

where:

$$\begin{aligned} Ne_i(c) &= \textstyle\int_0^{2\pi} Ce_i(c,v) Ce_i(c,v) dv; \\ Ae_{r,i} &= \textstyle\int_0^{2\pi} Ce_r(c_d,v) Ce_i(c,v) dv \end{aligned}$$

$$R1_r^{TM} = \left[Re_r^{(1)}(c_d,u_2) - \frac{Re_r^{(1)}(c_d,u_1)}{Re_r^{(2)}(c_d,u_1)} Re_r^{(2)}(c_d,u_2)\right]$$

Likewise, using boundary condition (10), one has

$$\begin{aligned} &\left(Ce_i(c,v_0) Re_i^{'(4)}(c,u_2) Re_i^{(4)}(c,u_0)\right) + \\ &X_i^{TM} Re_i^{'(4)}(c,u_2) Ne_i(c) = \sum_{r=0}^{\infty} P_r^{TM} Ae_{r,i} R1_r^{'TM} \end{aligned} \tag{18}$$

with $R1_r^{'TM} = \left[Re_r^{'(1)}(c_d,u_2) - \frac{Re_r^{(1)}(c_d,u_1)}{Re_r^{(2)}(c_d,u_1)} Re_r^{'(2)}(c_d,u_2)\right]$.

After subtracting the result of multiplying (17) by $Re_i^{'(4)}(c,u)$ and (18) by $Re_i^{(4)}(c,u)$, one gets' instead of 'one may subtract to get

$$\begin{aligned} &\sum_{r=0}^{\infty} P_r^{TM} Ae_{r,i}\left(Re_i^{'(4)}(c,u_2) R1_r^{TM} - R1_r^{'TM} Re_i^{(4)}(c,u_2)\right) \\ &= Ce_i(c,v_0) Re_i^{(4)}(c,u_0)\left(\begin{aligned} &Re_i^{(1)}(c,u_2) Re_i^{'(4)}(c,u_2) - \\ &Re_i^{'(1)}(c,u_2) Re_i^{(4)}(c,u_2) \end{aligned}\right) \end{aligned} \tag{19}$$

(19) can be re written as,

$$[P]\,[M] = [B] \tag{20}$$

$$B_i^{TM} = Ce_i(c, v_0) Re_i^{(4)}(c, u_0) \begin{bmatrix} Re_i^{(1)}(c, u_2) Re_i^{'(4)}(c, u_2) \\ -Re_i^{'(1)}(c, u_2) Re_i^{(4)}(c, u_2) \end{bmatrix}$$

And $M_{i,r}^{TM} = Ae_{r,i}\left(Re_i^{'(4)}(c, u_2) R1_r^{TM} - R1_r^{'TM} Re_i^{(4)}(c, u_2)\right)$.

The unknown coefficient P^{TM} is retrieved using the aforementioned relation, and X_i^{TM} is produced by inserting it in Equation (18). The same procedures are used with the odd part of Mathieu functions to extract the solution for Y_i^{TM}.

$$[S]\,[N] = [C] \tag{21}$$

where,

$$N_{i,r}^{TM} = Ao_{r,i}\left(Ro_i^{'(4)}(c, u_2) R2_r^{TM} - R2_r^{'TM} Ro_i^{(4)}(c, u_2)\right)$$

$$C_i^{TM} = So_i(c, v_0) Ro_i^{(4)}(c, u_0) \begin{bmatrix} Ro_i^{(1)}(c, u_2) Ro_i^{'(4)}(c, u_2) \\ -Ro_i^{'(1)}(c, u_2) Ro_i^{(4)}(c, u_2) \end{bmatrix}$$

$$Ao_{r,i} = \int_0^{2\pi} So_r(c_d, v) So_i(c, v) dv$$

$$R2_r^{TM} = \left[Ro_r^{(1)}(c_d, u_2) - \frac{Ro_r^{(1)}(c_d, u_1)}{Ro_r^{(2)}(c_d, u_1)} Ro_r^{(2)}(c_d, u_2) \right]$$

$$R2_r^{'TM} = \left[Ro_r^{'(1)}(c_d, u_2) - \frac{Ro_r^{(1)}(c_d, u_1)}{Ro_r^{(2)}(c_d, u_1)} Ro_r^{'(2)}(c_d, u_2) \right]$$

It is possible to determine the value of Y_i by knowing S. Therefore, the RCS of the covered metamaterial cylinder is computed using X_i and Y_i as follows:

$$\text{RCS} = \frac{16\pi^2}{k_0} \left[\sum_{i=0}^{\infty} j^i X_i^{TM} Ce_i(c, v) + \sum_{i=1}^{\infty} j^i Y_i^{TM} So_i(c, v) \right] \tag{22}$$

After computing Mathieu functions, using elliptical parameters the RCS of elliptic cylinder is determined.

3. RCS FOR COATED ELLIPTIC CYLINDER (CEC) USING DIFFERENT METAMATERIALS

Another way to express Equations (7) and (8) is as follows:

$$E_z^s = \left(\sum_{i=-0}^{\infty} B_{ei} Ce_i(c_0, v) Re_i^{(4)}(c_0, u) + \sum_{i=0}^{\infty} B_{oi} So_i(c_0, v) Ro_i^{(4)}(c_0, u) \right) \tag{23}$$

$$E_z^l = \left(\sum_{i=-0}^{\infty} C_{ei} Ce_i(c_1, v) Re_i^{(1)}(c_1, u) + \sum_{i=0}^{\infty} C_{oi} So_i(c_1, v) Ro_i^{(1)}(c_1, u) \right) \tag{24}$$

where $c_1 = k_1 F$ in which F is defined in the homogeneous wave equation (Helmholtz) in elliptical coordinates; c_1 is complex; and $k_1 = \omega\sqrt{\mu_1 \varepsilon_1}$, in which $\varepsilon_1 = \varepsilon'_1 - j\varepsilon''_1$; C_{ei} and C_{oi} are the expansion coefficients of the transmitted field that are unknown. Maxwell's equations can be used to determine the magnetic field component both within and outside the cylinder, i.e.,

$$H_u = \frac{j}{\omega\mu_1 h} \frac{\partial E_z}{\partial v} \tag{25}$$

$$H_v = \frac{j}{\omega\mu_1 h} \frac{\partial E_z}{\partial u} \tag{26}$$

$$h = F\sqrt{\text{coh}^2 u - \cos^2 v} \tag{27}$$

Imposing the continuity of the tangential field components at the cylinder's surface $u = u_1$ will yield the unknown expansion coefficients, i.e.,

$$\begin{aligned} &\sum_{i=0}^{\infty} M_{ei}(c_1, c_0) B_{ei} \left[\mu_r Re_{ei}^{(4)}(c_0, u_1) - \frac{Re_i^{(1)'}(c_1, u_1)}{Re_i^{(1)}(c_1, u_1)} Re_{ei}^{(4)}(c_0, u_1) \right] \\ &= \sum_{i=0}^{\infty} M_{ei}(c_1, c_0) A_{ei} \left[\frac{Re_i^{(1)'}(c_1, u_1)}{Re_i^{(1)}(c_1, u_1)} Re_{ei}^{(1)}(c_0, u_1) - \mu_r Re_{ei}^{(4)'}(c_0, u_1) \right] \end{aligned} \tag{28}$$

$$\begin{aligned} &\sum_{i=1}^{\infty} M_{oi}(c_1, c_0) B_{oi} \left[\mu_r Re_{ei}^{(4)'}(c_0, u_1) - \frac{Re_i^{(1)'}(c_1, u_1)}{Re_i^{(1)}(c_1, u_1)} Re_{oi}^{(4)}(c_0, u_1) \right] \\ &= \sum_{i=0}^{\infty} M_{oi}(c_1, c_0) A_{oi} \left[\frac{Re_i^{(1)'}(c_1, u_1)}{Re_i^{(1)}(c_1, u_1)} Re_{oi}^{(1)}(c_0, u_1) - \mu_r Re_{ei}^{(1)'}(c_0, u_1) \right] \end{aligned} \tag{29}$$

$$M_{\substack{ei\\oi}}(c_0, c_1) = \int_0^{2\pi} S_{\substack{ei\\oi}}(c_1, \eta) S_{\substack{ei\\oi}}(c_0, \eta) \tag{30}$$

where the dielectric region's relative permeability is denoted by μr. Additionally shown is the TE scattering by a lossy elliptic cylinder. The following answer is obtained in this instance using a derivation due to that of the TM case [14].

$$\begin{aligned}&\sum_{i=0}^{\infty} M_{ei}(c_1,c_0)B_{ei}^{TE}\left[\varepsilon_r Re_{ei}^{(4)'}(c_0,u_1)\right.\\&\left.\qquad-\frac{Re_i^{(1)'}(c_d,u_1)}{Re_i^{(1)}(c_d,u_1)}Re_{ei}^{(4)}(c_0,u_1)\right]\\&=\sum_{i=0}^{\infty} M_{ei}(c_1,c_0)A_{ei}\left[\frac{Re_i^{(1)'}(c_d,u_1)}{Re_i^{(1)}(c_d,u_1)}Re_{ei}^{(1)}(c_0,u_1)\right.\\&\left.\qquad-\varepsilon_r Re_{ei}^{(1)'}(c_0,u_1)\right]\end{aligned}\tag{31}$$

$$\begin{aligned}&\sum_{i=0}^{\infty} M_{oi}(c_1,c_0)B_{oi}^{TE}\left[\varepsilon_r Re_{oi}^{(4)'}(c_0,u_1)\right.\\&\left.\qquad-\frac{Re_i^{(1)'}(c_1,u_1)}{Re_i^{(1)}(c_1,u_1)}Re_{ei}^{(4)}(c_0,u_1)\right]\\&=\sum_{i=0}^{\infty} M_{ei}(c_1,c_0)A_{ei}\left[\frac{Re_i^{(1)'}(c_1,u_1)}{Re_i^{(1)}(c_1,u_1)}Re_{ei}^{(1)}(c_0,u_1)\right.\\&\left.\qquad-\varepsilon_r Re_{ei}^{(1)'}(c_0,u_1)\right]\end{aligned}\tag{32}$$

Once the scattered field expansion coefficients are determined, the scattered near and distant fields for the TM and TE cases may be computed. The following outlines the method used to drive the far scattered field expressions:

$$E_z^s=\sqrt{\frac{j}{k_0\rho}}e^{-jk_0\rho}\sum_i j^i[B_{ei}^{TM}S_{ei}(c_0,\eta)+B_{oi}^{TM}S_{oi}(c_0,\eta)] \tag{33}$$

$$H_z^s=\sqrt{\frac{j}{k_0\rho}}e^{-jk_0\rho}\sum_i j^i[B_{ei}^{TE}S_{ei}(c_0,\eta)+B_{oi}^{TE}S_{oi}(c_0,\eta)] \tag{34}$$

The echo width, or scattering cross section per unit length, is typically used to express far-field data. It is defined as follows for the TM polarization case:

$$\sigma_{TM}=2\pi\rho\lim_{\rho\to\infty}\frac{|E_z^s|^2}{|E_z^i|^2} \tag{35}$$

For computational purposes, Eq. (34) can be expressed in the following simpler form:

$$\sqrt{\frac{\sigma_{TM}}{\lambda}}=\sum_i j^i[B_{ei}S_{ei}(c_0,\eta)+B_{oi}S_{oi}(c_0,\eta)] \tag{36}$$

The electrical permittivity and magnetic permeability values listed in Table 1 can be used to categorize metamaterials. RCS is obtained by substituting these values into Equations (28)–(32).

4. RCS FOR COVERED ELLIPTIC CONE (CECO) BY METAMATERIALS

With the use of the spheroconal coordinates [15], which are defined by the scatterer's geometry (Fig. 3),

$$x=r\sin\theta\cos\phi \qquad 0\le r<\infty$$

$$y=r\sqrt{1-k^2\cos^2\theta\sin\phi} \qquad 0\le\theta\le\pi,\ 0\le\phi\le 2\pi$$

$$z=r\cos\theta\sqrt{1-k'^2\sin^2\phi} \qquad 0<k,k'\le 1,\ k^2+k'^2=1.$$

It is possible for the incident plane wave to travel in the positive z-direction. Its vectors of fields are

$$E_i = a_x E_0 e^{-j\beta a_z\cdot r} \tag{37}$$

$$H_i = a_y H_0 e^{-j\beta a_z\cdot r} \qquad H_0=\frac{E_0}{Z_0} \tag{38}$$

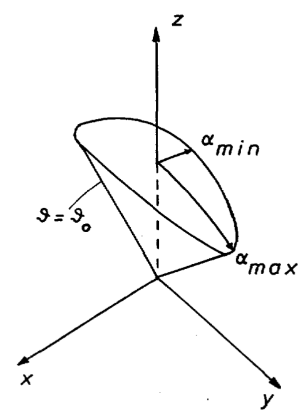

FIGURE 3. Elliptic cone geometry.

The scattered field's physical optics approximation in the far zone can be expressed as [2].

$$E_{SC}=\frac{e^{-j\beta r}}{r}\frac{j\omega\mu_0}{2\pi}\iint_A a_0\times[a_0\times(a_\theta\times H_0a_y)e^{-j\beta(a_z-a_0)\cdot r}da] \tag{39}$$

where a_θ is the normal unit vector on the cone surface, A the cone surface, and a_0 the unit vector in the observation direction. We must select $a_0=-a_z$ in order to calculate the backscattering cross section. In this instance, (3) produces

$$\begin{aligned}E_{SC} &= \Gamma\frac{e^{-j\beta r}}{r}\frac{j\omega\mu_0}{2\pi}[-H_0\sqrt{1-k^2\cos^2\theta_0}.\sin\theta_0]a_x\\&\int_0^{2\pi}\int_0^{\infty} r'e^{-j\beta\zeta r'}dr'd\theta\end{aligned}\tag{40}$$

$$\zeta = \sqrt{1-k'\sin^2\phi'}\cos\theta_0 \tag{41}$$

Calculate integration over r'.

Γ is the reification coefficient, and if β is a real number, then this expression does not converge for $r\to\infty$. The medium around the cone is therefore thought to be lossy. In this instance, the right side of (5) for $r\to\infty$ is forced to converge due to β

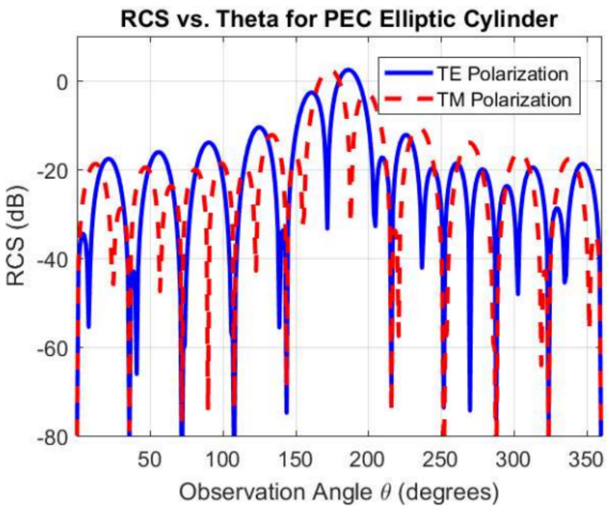

FIGURE 4. RCS for PEC elliptic cylinder-uncovered (TE and TM polarizations).

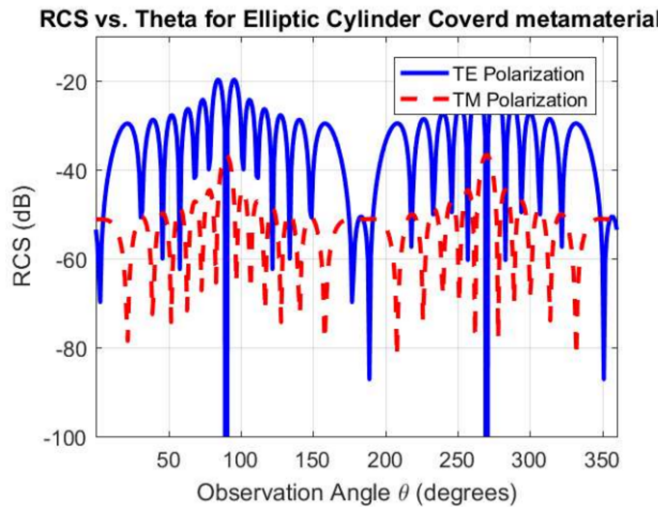

FIGURE 5. RCS for covered metamaterial elliptic cylinder (TE and TM polarizations) ($f = 1$ GHz).

negative imaginary portion. Let β fictitious half disappear now. It is easy to perform the remaining integral over (ϕ'), and the field that results in is

$$E_{SC} = \Gamma \frac{e^{-j\beta r}}{r} \frac{j\omega\mu_0}{4\beta^2 k} H_0 \frac{\sqrt{1-k^2\cos^2\theta_0}\sin\theta_0}{\cos^2\theta_0} a_x \quad (42)$$

The starting point for computing the backscattering cross-section is given by:

$$\text{RCS} = \lim_{r\to\infty} 4\pi r^2 \frac{|S_{SC}|}{|S_i|} \quad (43)$$

where S denotes the time averaged Poynting vector

$$|S_{SC}| = \frac{1}{2Z_0} |E_{SC}|^2 \quad (44)$$

$$|S_i| = \frac{1}{2} Z_0 H_0^2 \quad (45)$$

Obtain:

$$\text{RCS} = \Gamma \frac{\lambda^2}{16\pi k} \frac{(1-k^2\cos^2\theta_0)\sin^2\theta_0}{\cos^4\theta_0} \quad (46)$$

with λ being the wavelength. If the incident plane wave is polarized ordinarily to that taken into consideration, the same formula yields the same answer. The extreme flare angles α_{min} and α_{max} (Fig. 3) of the cone, which are connected to k and θ_0, can be expressed in terms of Equation (46) by:

$$\alpha_{\text{min}} = \theta_0 \ . \quad \text{and} \quad \cos\alpha_{\text{max}} = k\cos\theta_0$$

The result obtained is:

$$\text{RCS} = \Gamma \frac{\lambda^2}{16\pi} \tan^2\alpha_{\text{min}} \tan^2\alpha_{\text{max}} \quad (47)$$

From above equation RCS for circular cone in case $\alpha_0 = \alpha_{\text{min}} = \alpha_{\text{max}}$

$$\text{RCS} = \Gamma \frac{\lambda^2}{16\pi} \tan^4\alpha_0 \quad (48)$$

For normal, TE and TM incident Γ are given as:

$$\Gamma = \frac{Z_d - Z_0}{Z_d + Z_0} \quad (49)$$

$$\Gamma_{TE} = \frac{Z_d\cos\theta_i - Z_0\cos\theta_t}{Z_d\cos\theta_i + Z_0\cos\theta_t} \quad (50)$$

$$\Gamma_{TM} = \frac{Z_d\cos\theta_t - Z_0\cos\theta_i}{Z_d\cos\theta_t + Z_0\cos\theta_i} \quad (51)$$

5. RESULTS AND DISCUSSIONS

A PEC elliptical cylinder's RCS is depicted in Fig. 4, and Fig. 5 shows the same cylinder with a single layer of metamaterials applied. Its properties are as permittivity $= 10$, permeability $= -1$ (MNG metamaterial) with thickness equal to 0.01 m. When comparing the two figures, we can see that the coated cylinder's radar value has decreased.

At a frequency of 3 GHz for TE and TM polarizations, Fig. 6 displays the RCS of an elliptical cylinder coated with a metamaterial whose characteristics are permittivity $= 4 - j$, permeability $= 2 - 0.5j$ for varying values of the angle of incidence at $\phi_{inc} = 0, \;\; 45 \quad and 90$. The fact that RCS levels for the two scenarios are similar indicates that the metamaterial is effective at lowering radar.

RCS of an elliptical cylinder covered in metamaterial is depicted in Fig. 7, and its properties are as permittivity $= 4 - 0.2j$, permeability $= 1 - 0.1j$ at a frequency of 3 GHz for varying metamaterial layer thicknesses. It is observed that in the case of TE polarization, RCS fluctuates with thickness, but in the case of TM polarization, the thickness has no influence.

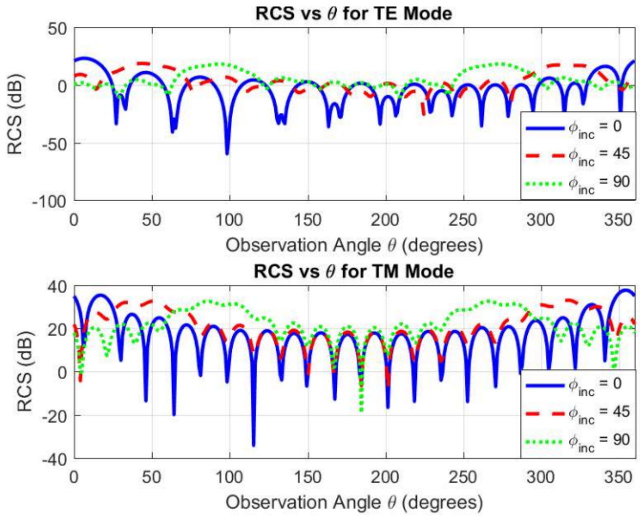

FIGURE 6. RCS for covered metamaterial elliptic cylinder (TE and TM polarizations) for varying incidence angle values.

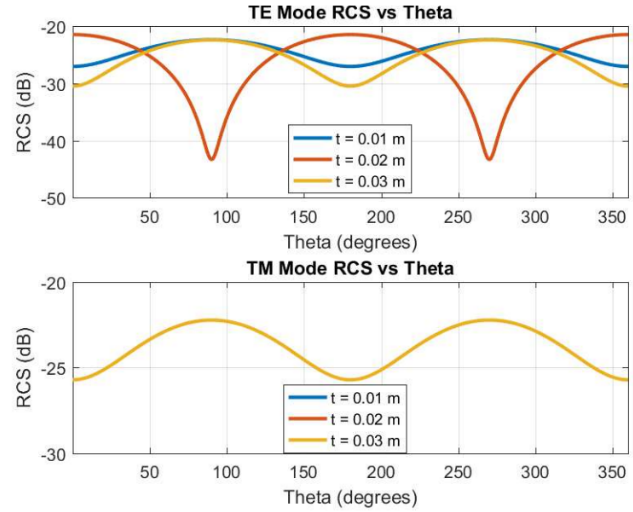

FIGURE 7. RCS for covered metamaterial elliptic cylinder (TE and TM polarizations) for varying thicknesses.

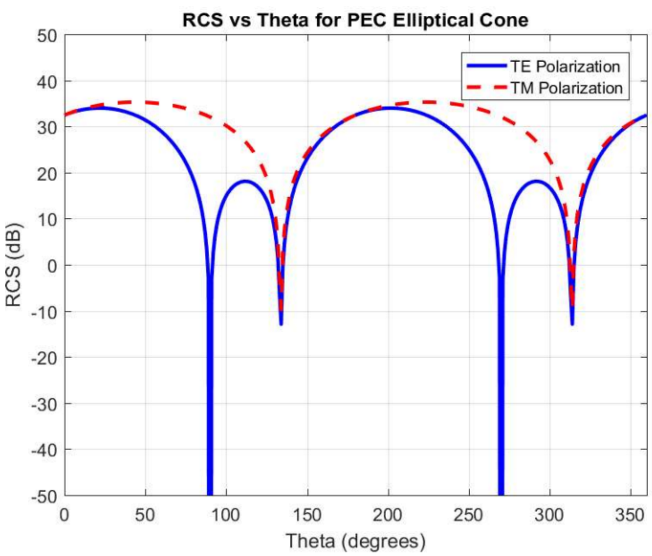

FIGURE 8. RCS for PEC elliptic cone-uncovered (TE and TM polarization).

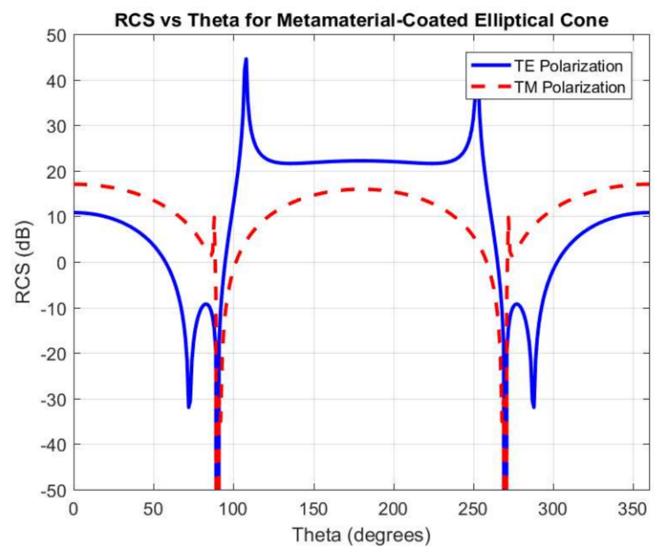

FIGURE 9. RCS for covered metamaterial elliptic cone (TE and TM polarizations) ($f = 1$ GHz).

A PEC elliptical cone RCS is depicted in Fig. 8, and Fig. 9 shows the same cone with a single layer of metamaterials applied. Its properties are as permittivity $= 10$, permeability $= -1$ (MNG metamaterial) with thickness equal to 0.01 m. When comparing the two Figures, we can see that the coated cone radar value has decreased at TE polarization about 20 dB, and decreased about 15 dB in TM polarization.

Figure 10 shows the RCS of an elliptical cone coated with a metamaterial whose properties are permeability $= 2-0.5j$, permittivity $= 4 - j$ for different values of the angle of incidence at $\phi_{inc} = 0$, 45, and 90 at a frequency of 3 GHz for TE and TM polarizations. The effectiveness of the metamaterial in reducing radar is demonstrated by similar RCS values for the two cases. Fig. 11 shows the RCS of an elliptical cone coated with metamaterial. For different metamaterial layer thicknesses, the characteristics are as follows: permeability $= 1-0.1j$, permittivity $= 4 - 0.2j$, at a frequency of 3 GHz. RCS is found to vary with thickness in the case of TE and TM polarizations,

Furthermore, Fig. 11 demonstrates that the thickness of the metamaterial generated decreases as RCS decreases, suggesting that the thickness of the metamaterial must be increased while taking its weight into consideration.

Additionally, in Fig. 7 as the thickness of the metamaterial increases, the RCS decreases, which highlights the importance of increasing the metamaterial's thickness while considering its weight.

6. RESULTS OF RCS FOR ELLIPTIC CYLINDER AND ELLIPTIC CONE

The RCS of objects consisting of multiple components can be determined using superposition theory. In this study, the RCS

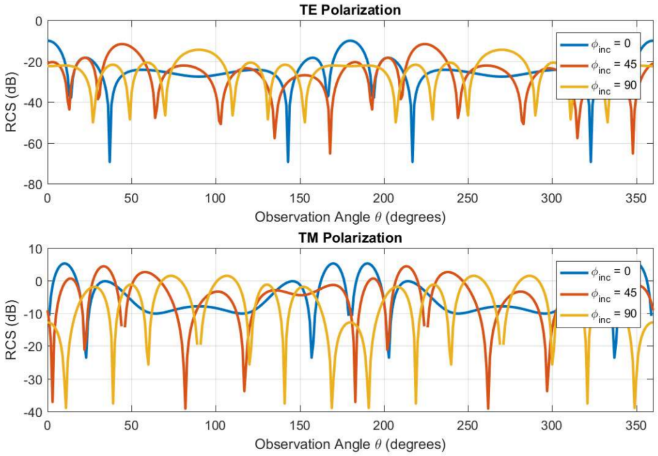

FIGURE 10. RCS for covered metamaterial elliptic cone (TE and TM polarizations) for varying incidence angle values.

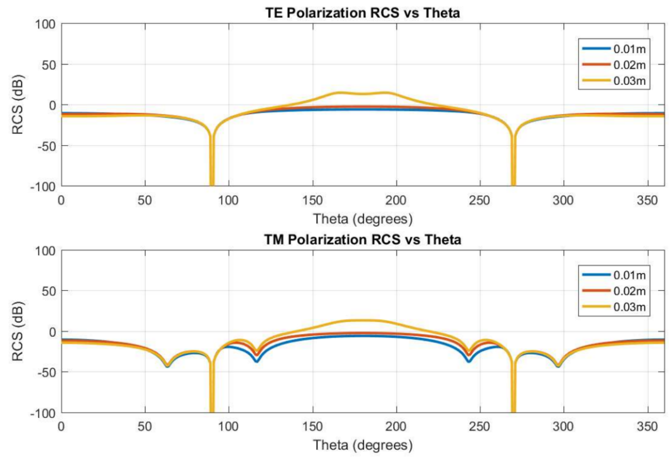

FIGURE 11. RCS for covered metamaterial elliptic cone (TE and TM polarizations) for varying thicknesses.

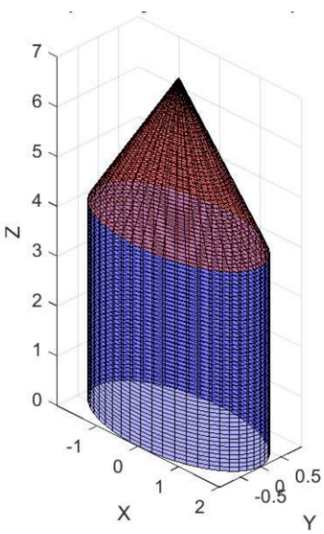

FIGURE 12. The problem's geometric for PEC target.

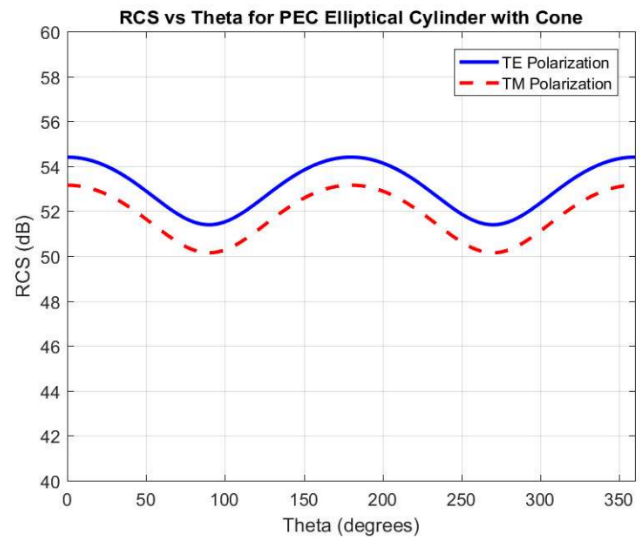

FIGURE 13. RCS for PEC shape (TE and TM polarizations).

equation is derived for each part independently, and the equations are combined to obtain the overall RCS. RCS for the elliptical cylinder is discovered in this work, followed by RCS for the elliptical cone. In this section, RCS will be located by using the superposition theory for Equations (22) and (47) to the target depicted in Fig. 12.

Figure 13 displays RCS for the PEC-based target, and Fig. 14 displays the same target with a layer of designed metamaterials from [12] applied, which has the following properties (permittivity $= 3.45 - 23.108j$, permeability $= -1.59 - 24.36j$, at $f = 2$ GHz for TE) and (permittivity $= -45.74 - 10.185j$, permeability $= 12.63 - 2.53j$, at $f = 2$ GHz for TM). It is evident from comparing the two figures that the addition of a layer of metamaterials to the target reduced RCS. For instance at the angle of incidence Zero RCS decreased by about 42 dB.

The study's validity is further supported by Fig. 14, which displays the consistency between the outcomes from the Computer Simulation Technology (CST) simulation program and the equations.

Figure 15 shows the RCS of target coated with designed metamaterial [12] whose properties are permittivity $= 1.282 - 5.0121j$, permeability $= 0.746 - 4.52j$, at $f = 10$ GHz for TE and permittivity $= 0.942 - 3.88j$, permeability $= 1.087 - 5.859j$, at $f = 10$ GHz for TM for different values of the angle of incidence at ($\phi_{inc} = 0,\ \ 45 \quad and 90$) at a frequency of 1 GHz for TE and TM polarizations. The effectiveness of the metamaterial in reducing radar is demonstrated by the similar RCS values for the two cases.

Figures 16 and 17 shows the RCS of target coated in metamaterial designed [12]. For different metamaterial layers, the characteristics are permittivity $= 0.9935 - 0.4757j$, permeability $= 1.0047 - 0.4787j$, at $f = 100$ GHz for TE and permittivity $= 0.9897 - 0.4732j$, permeability $= 1.0105 - 0.4811j$, at $f = 100$ GHz for TM. RCS is found to vary little when change layers in the case of TE polarization and TM polarization. Furthermore, Fig. 16 and Fig. 17 illustrate that the number of designed metamaterial layers increased as RCS decreased, suggesting that metamaterial layers must be increased while its weight is taken into consideration.

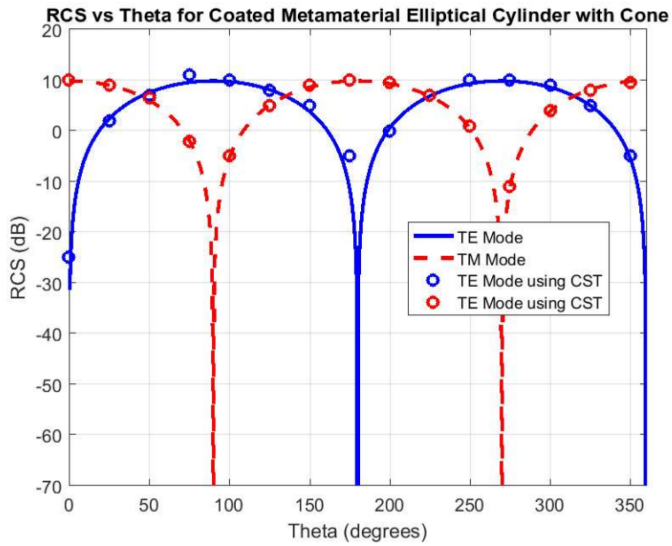

FIGURE 14. RCS for covered metamaterial target (TE and TM polarizations) ($f = 2$ GHz).

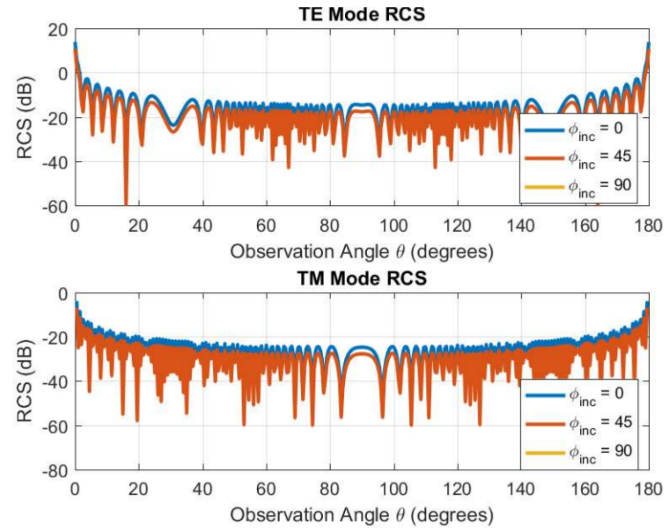

FIGURE 15. RCS for covered metamaterial target (TE and TM polarizations) for varying incidence angle values ($f = 100$ GHz).

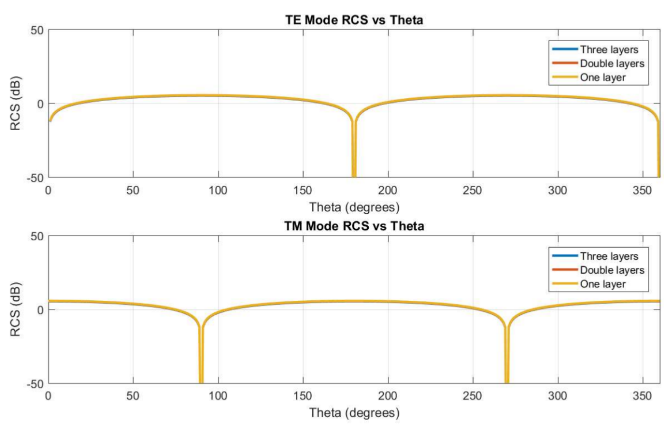

FIGURE 16. RCS for covered metamaterial target (TE and TM polarizations) for varying thicknesses.

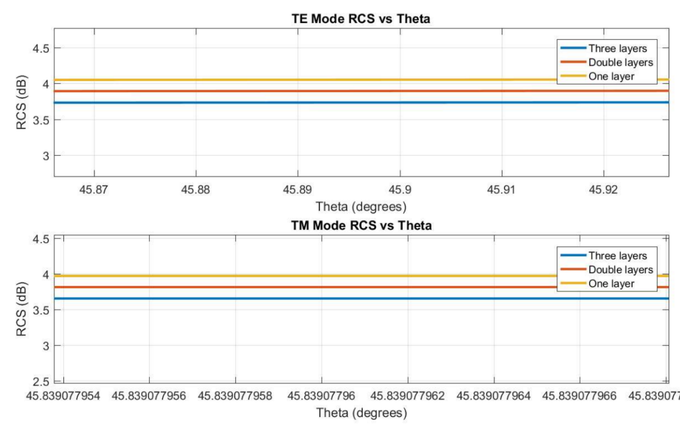

FIGURE 17. A tiny section of Fig. 16.

7. CONCLUSION

RCS was determined for the elliptical cylinder and elliptical cone in the two scenarios where they were coated with metamaterials and made from a highly conductive material (PEC) after the scattering was computed using the Mathieu function. RCS was calculated using the principle of superposition for an object consisting of a cylinder and a cone when the body was composed of a well-conductive material (PEC) and when the body was coated with metamaterials.

The RCS decreased by almost 42 dB at 2 GHz when the target was covered with the designed metamaterial.

Additionally, the RCS dropped to below zero when the designated metamaterial was added at 10 GHz and at different angles of incidence.

At 100 GHz, the difference among one layer, two layers, and three layers is not statistically significant, but the RCS decreases as the number of layers in the intended metamaterial increases.

REFERENCES

[1] Wait, J. R., "Scattering of a plane wave from a circular dielectric cylinder at oblique incidence," *Canadian Journal of Physics*, Vol. 33, No. 5, 189–195, 1955.

[2] Wang, N., "Electromagnetic scattering from a dielectric-coated circular cylinder," *IEEE Transactions on Antennas and Propagation*, Vol. 33, No. 9, 960–963, 1985.

[3] Bowman, J., T. Senior, and P. Uslenghi, "The wedge," *Electromagnetic and Acoustic Scattering by Simple Shapes*, 252–283, 1969.

[4] Yeh, C., "Backscattering cross section of a dielectric elliptical cylinder," *Journal of the Optical Society of America*, Vol. 55, No. 3, 309–314, 1965.

[5] Richmond, J. H., "Scattering by a conducting elliptic cylinder with dielectric coating," *Radio Science*, Vol. 23, No. 06, 1061–1066, 1988.

[6] Sebak, A.-R., "Scattering from dielectric-coated impedance elliptic cylinder," *IEEE Transactions on Antennas and Propagation*, Vol. 48, No. 10, 1574–1580, 2000.

[7] Caorsi, S., M. Pastorino, and M. Raffetto, "Electromagnetic scattering by a multilayer elliptic cylinder under transverse-magnetic illumination: Series solution in terms of Mathieu functions," *IEEE Transactions on Antennas and Propagation*, Vol. 45, No. 6, 926–935, 1997.

[8] Ragheb, H. A., L. Shafai, and M. Hamid, "Plane wave scattering by a conducting elliptic cylinder coated by a nonconfocal dielectric," *IEEE Transactions on Antennas and Propagation*, Vol. 39, No. 2, 218–223, 1991.

[9] Abramowitz, M. and I. A. Stegun, *Handbook of Mathematical Functions with Formulas, Graphs, and Mathematical Tables*, US Government Printing Office, 1948.

[10] Siegel, K. M., J. W. Crispin, and C. E. Schensted, "Electromagnetic and acoustical scattering from a semi-infinite cone," *Journal of Applied Physics*, Vol. 26, No. 3, 309–313, 1955.

[11] Blume, S. and G. Kahl, "The physical optics radar cross section of an elliptic cone," *IEEE Transactions on Antennas and Propagation*, Vol. 35, No. 4, 457–460, 1987.

[12] Alsemaid, O. M., A. A. Babiker, and E. S. Saad, "Design and analysis of multi-layer resistive ink film based metamaterial ultra-thin broadband absorber," *International Journal of Computing and Engineering*, Vol. 5, No. 4, 27–43, 2024.

[13] Manmohan, C. T., R. U. Nair, and H. Singh, "Radar cross section of a coated elliptic cylinder using addition theorem," in *2016 International Symposium on Antennas and Propagation (APSYM)*, 1–4, Cochin, India, Dec. 2016.

[14] Hussein, M. I. and A. K. Hamid, "Electromagnetic scattering by a lossy dielectric elliptic cylinder," *Journal of Electromagnetic Waves and Applications*, Vol. 15, No. 11, 1469–1482, 2001.

[15] Blume, S. and G. Kahl, "Field singularities at the tip of a cone elliptic cross section," *Optik (Stuttgart)*, Vol. 70, No. 4, 170–175, 1985.